Research Paper

Localized delivery of curcumin into brain with polysorbate 80-modified cerasomes by ultrasound-targeted microbubble destruction for improved Parkinson's disease therapy

Nisi Zhang[#,1,2], Fei Yan[#,2], Xiaolong Liang[1], Manxiang Wu[2,3], Yuanyuan Shen[4], Min Chen[1], Yunxue Xu[1], Guangyang Zou[1], Peng Jiang[2], Caiyun Tang[2], Hairong Zheng[2✉], Zhifei Dai[1✉]

1. Department of Biomedical Engineering, College of Engineering, Peking University, Beijing, 100871, China.
2. Paul C. Lauterbur Research Center for Biomedical Imaging, Institute of Biomedical and Health Engineering, Shenzhen Institutes of Advanced Technology, Chinese Academy of Sciences, Shenzhen, 518055, China.
3. Department of Medicine Ultrasonics, Nanfang Hospital, Southern Medical University, Guangzhou, China.
4. School of Biomedical Engineering, Shenzhen University, Shenzhen, 518060, China.

\# These authors contributed equally to this work.

✉ Corresponding authors: Z.D. (Email: zhifei.dai@pku.edu.cn) and H. Z. (Email: hr.zheng@siat.ac.cn)

Abstract

Rationale: Treatment for Parkinson's disease (PD) is challenged by the presence of the blood-brain barrier (BBB) that significantly limits the effective drug concentration in a patient's brain for therapeutic response throughout various stages of PD. Curcumin holds the potential for α-synuclein clearance to treat PD; however, its applications are still limited due to its low bioavailability and poor permeability through the BBB in a free form.

Methods: Herein, this paper fabricated curcumin-loaded polysorbate 80-modified cerasome (CPC) nanoparticles (NPs) with a mean diameter of ~110 nm for enhancing the localized curcumin delivery into the targeted brain nuclei via effective BBB opening in combination with ultrasound-targeted microbubble destruction (UTMD).

Results: The liposomal nanohybrid cerasome exhibited superior stability towards PS 80 surfactant solubilization and longer circulation lifetime ($t_{1/2}$ = 6.22 h), much longer than free curcumin ($t_{1/2}$ = 0.76 h). The permeation was found to be 1.7-fold higher than that of CPC treatment only at 6 h after the systemic administration of CPC NPs. Notably, motor behaviors, dopamine (DA) level and tyrosine hydroxylase (TH) expression all returned to normal, thanks to α-synuclein (AS) removal mediated by efficient curcumin delivery to the striatum. Most importantly, the animal experiment demonstrated that the 1-methyl-4-phenyl-1,2,3,6-tetrahydropyridine (MPTP)-induced PD mice had notably improved behavior disorder and dopamine depletion during two-week post-observation after treatment with CPC NPs (15 mg curcumin/kg) coupled with UTMD.

Conclusion: This novel CPC-UTMD formulation approach could be an effective, safe and amenable choice with higher therapeutic relevance and fewer unwanted complications than conventional chemotherapeutics delivery systems for PD treatment in the near future.

Key words: curcumin, Parkinson's disease, blood-brain barrier, cerasome, ultrasound targeting microbubbles destruction

Introduction

Parkinson's disease (PD) is one of the most severe and refractory age-related motoric neurodeg-enerative diseases [1]. It pathologically originates from the progressive death of midbrain dopaminergic

neurons of substantia nigra pars compacta (SNC) and the deposition of misfolded α-synuclein (AS) aggregates [2, 3]. Deep brain stimulation (DBS) [4] and transplantation of fetal dopamine neurons [5, 6] can improve the clinical state of PD patients but these approaches remain unsatisfying due to their complex and painful surgical procedures [7], high cost and severe side effects [8, 9]. There are also other advancing clinical trials for PD patients, such as focused ultrasound subthalamotomy, which is a thermal ablation treatment that causes irreversible subthalamic nucleus destruction [10]. Among all medical treatment options for PD, pharmacotherapy is vital to alleviate the symptoms of this neurodege-nerative diseases [11]. Yet, many potential PD pharmacological agents have no or limited therapeutic efficacies due to their inability or low efficiency in penetrating the blood-brain barrier (BBB) [12]. Therefore, there is a pressing demand to find practical strategies for the delivery of these pharmaceuticals in vivo through the BBB without disrupting the brain's functioning [13].

In recent years, various physical and chemical treatment methods have been explored to circumvent or cross the BBB [14-20]. Especially, a variety of drug delivery systems based on nanoparticles (NPs) have been explored to cross the BBB. Ideal nanocarriers for the central nervous system (CNS) should be able to accumulate in the CNS upon systemic administration, permeate the BBB, precisely target a specific group of cells in the CNS, and then release the drug cargo, resulting in minimal systemic effects. Polysorbate 80 (PS 80), an excipient and surfactant, has widely been used in the clinic to stabilize aqueous formulations of medications for parenteral administration [21] or used as an emulsifier in manufacturing [22] due to its amphiphilicity and low toxicity. More interestingly, PS 80 was explored to modify the surface of nanocarriers for the delivery of a number of CNS drugs into the brain of animals with varying success [23-25]. These strategies involve serum ApoE adsorption onto the particles, thus causing interact-tions with low-density lipoprotein receptor-related protein 1 (LRP1) followed by transcytosis across the BBB through vascular endothelial cells [25]. However, PS 80 may induce the destabilization of the nanocarriers (e.g., liposomes), resulting in accelerated and premature drug release during circulation. In addition, PS 80-mediated BBB permeability is unspecific and lacks localized drug delivery capabil-ities, which largely increase the risk of potential side effects [26].

Ultrasound-targeted microbubble destruction (UTMD) is advantageous for delivering drugs across the BBB into a localized brain tissue or nuclei via the cavitation effect [27]. In a first-in-human trial in 2016, Carpentier et al. developed an ultrasound device implanted into the skull of patients, and used UTMD for the treatment of glioblastoma [28]. It has been shown that low-intensity pulsed focused ultrasound can transcranially enter the brain and induce transient and reversible separation of endothelial tight junctions in the presence of microbubbles (MBs) [29-32]. Such UTMD-induced BBB opening allows extravasation of large therapeutics (e.g., antibodies, growth factors, nanoparticles, nucleic acids) into the brain from the systemic circulation without pathology or entry of blood components [33-35]. Though not extensive currently, this strategy paves the way for treatment of neurodegenerative diseases in the near future.

Curcumin is neuroprotective in neurological disorders with continual and sufficient intake [36-38]. Several studies in different experimental PD models in vitro found that curcumin could inhibit and remove AS effectively, leading to attenuation of AS oligomer toxicity in cells [39, 40]. In addition, a considerable body of research confirmed that curcumin was non-toxic even at high doses [41-43]. However, curcumin possesses poor bioavailability due to its poor absorption, rapid metabolism and elimination, and poor permeability to the BBB [44, 45].

To overcome the above problems associated with the delivery of curcumin across the BBB for improved PD treatment, we herein fabricate curcumin-loaded PS 80-modified cerasomes (CPC). Hydrophobic curcumin molecules are present in the hydrophobic domain of the lipid bilayer of cerasomes [46-49]. The surface modification with PS 80 is used to assist the curcumin nanocarriers across the BBB by transcytosis through vascular endothelial cells [25]. Additionally, cerasome has a bilayer vesicular structure and a silicate surface with a molecular structure analogous to lipids, but possesses better morphological stability than conventional liposomes and endows better biocompatibility than silica nanoparticles. Hence, due to its superior stability towards PS 80 surfactant solubilization, the liposomal nanohybrid cerasome was selected as the curcumin nanocarrier [50-53]. In addition, with the assistance of the UTMD technique to induce BBB opening regionally and noninvasively, localized delivery of the CPC NPs into the mouse brain was achieved, causing improved therapeutic efficacy for PD (**Figure 1**).

Results

Preparation and characterization of the CPC nanoparticles

CPC NPs were prepared by addition of PS 80 to

the lipid-curcumin thin film at different weight ratios of PS 80/CFL using a thin-film hydration method in combination with sol-gel reaction and self-assembly process. **Table 1** shows the hydrodynamic diameters, zeta potentials, drug encapsulation efficiencies (EE) and drug loading contents (DLC). The addition of PS 80 had little effect on the particle size, and the hydrodynamic diameters of all CPC NPs with different PS 80 contents were about 110 nm. Additionally, the zeta potentials were -34.5 ± 2.9, -25.0 ± 0.9 and -16.5 ± 0.8 mV for curcumin cerasomes, 5% PS 80 CPC NPs and 10% PS 80 CPC NPs, respectively. 10% PS 80 CPC exhibited a lower absolute zeta potential than CPC with less PS 80, resulting in an increase in negative charge.

Table 1. The hydrodynamic diameters and zeta potentials of CPC NPs with different weight ratios of PS 80 to CFL. The data represent mean values for n=3.

PS 80 (%)	Particle size	PDI	Zeta potential (mV)	EE (%)	DLC (%)
0%	111.90±2.08	0.28	-34.5±2.9	46±0.38	2.98±0.03
5%	110.43±6.59	0.13	-25.0±0.9	86±1.25	5.42±0.08
10%	110.89±16.23	0.14	-16.5±0.8	87±0.13	5.48±0.01

The EE and DLC were evaluated by measuring curcumin absorbance at 414 nm. Quantitively, a curcumin EE of only 45.88% ± 0.38% was obtained when using pure cerasomes, but >80% was achieved when 5% or 10% of PS 80 were used in these formulations. The DLC was 2.98 ± 0.03%, 5.42 ± 0.08% and 5.48 ± 0.01% for curcumin cerasomes, 5% PS 80 CPC and 10% PS 80 CPC, respectively. The doubled EE and DLC may contribute to the surfactant effect of PS 80 to some extent. Significantly, the 5% PS 80 CPC showed a fairly uniform distribution and good shelf stability (**Figure 2A-B**), and no significant changes in particle size and zeta potential were observed within 4 weeks (**Figure 2C**). Also, the CPC NPs were analyzed by transmission electron microscopy (TEM; **Figure 2D** and **Figure S1**) and atomic force micros-copy (AFM; **Figure 2E-F**). As shown in **Figure 2F**, the CPC NPs appeared circular with varied surface thickness. Two-dimensional and three-dimensional AFM images further revealed that the particle actually maintained a spherical shape with rough surfaces.

CPC-releasing behavior *in vitro*, and pharmacokinetic profile and bio-distribution *in vivo*

The release of curcumin from the PS 80-ceras-omes is presented in **Figure 3A**. Notably, cerasomes containing 0%, 5% and 10% PS 80 released 46.4%, 51.1%, and 68.6% curcumin in the first 10 h, respectively. Clearly, the initial burst release of curcumin from cerasomes increased with PS 80 content, indicating that curcumin interacts more strongly with hydrolyzed CFLs than PS 80. Also, the sustained release of curcumin from cerasomes follow-ed the initial burst increased as the PS 80 content increased. As a result, the total release of curcumin from cera-somes containing 0%, 5%, and 10% PS 80 was 80.8%, 89.6%, and 98.6% in 60 h, respectively. The slower release rate for cerasomes was attributed to the siloxane networks that blocked the drug release channels.

The blood pharmacokinetics of CPC NPs were monitored in healthy C57BL/6 mice. The percentage of the injected dose in the blood (ID%) over time is shown in **Figure 3B**. Compared with free curcumin, the cerasomal curcumin displayed prolonged blood circulation time and higher blood concentrations at physiological temperatures (37 °C). The content of PS 80 was found to effect ID%. Approximately 76% ± 4% of curcumin for 5% PS 80 CPC and 72% ± 2% for 10% PS 80 CPC remained in the blood circulation at 1 h after administration, which was significantly lower than for curcumin
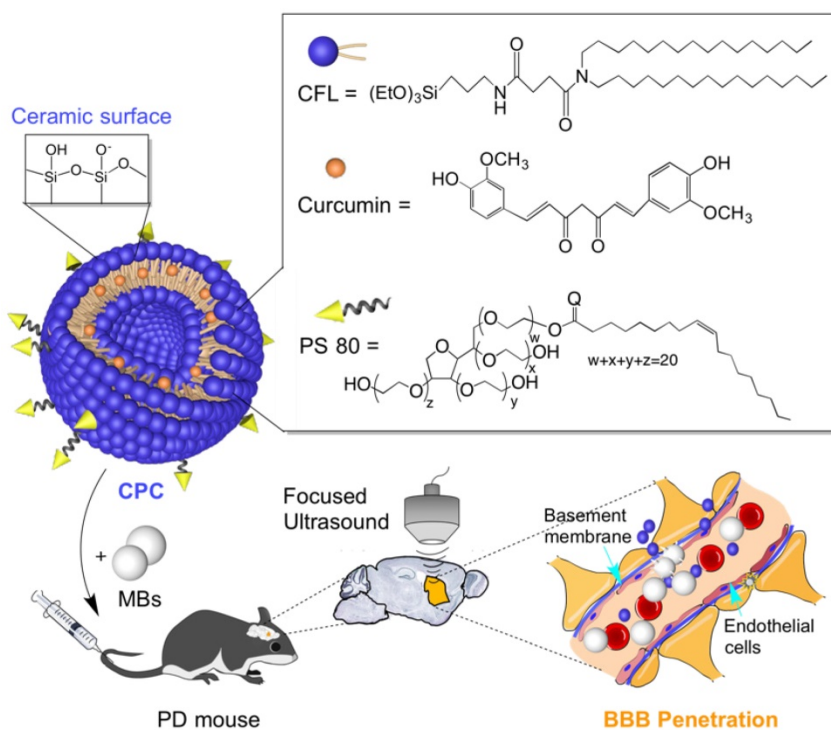

Figure 1. Improved therapeutic efficacy of curcumin in PD mice using CPC combined with UTMD. Schematic illustration of the CPC chemical composition and the noninvasive localized delivery of CPC NPs to the mouse brain by the UTMD technique for improved PD therapy.

cerasomes with no PS 80 (87% ± 5%). This was consistent with the in vitro drug release experiments. From the area under the plasma concentration time curve (AUC) for 0-24 h, the order of the half-life time ($t_{1/2}$) was evaluated to be 1636%, 937% and 706% ID h for curcumin cerasomes, 5% PS 80 CPC and 10% PS80 CPC, respectively. Despite some premature drug release from CPC, the curcumin in the vehicles still showed remarkably higher $t_{1/2}$ (11.05 h, 6.22 h, and 4.86 h for curcumin cerasomes and CPC with 5% or 10% PS 80, respectively) than the free curcumin (0.76 h). All these data above demonstrated that if modified with PS 80 to further explore the permeability of the particles, CPC NPs with 5% PS 80 had not only relatively high blood stability compared to the 10% PS 80 CPC particles, but also better drug loading capacity than curcumin cerasomes and significantly longer blood circulation time than free curcumin. Therefore, CPC NPs with 5% PS 80 were optimal for in vivo drug delivery so they were used for all the following studies.

In order to measure efficiency crossing the BBB, the in vivo biodistribution of CPC NPs was analyzed in healthy C57BL/6 mice by determining the curcumin fluorescence in the major organs over 24 h. Similar to that in the liver and kidneys, a gradual increase in curcumin could be observed in the brain after i.v. administration of CPC NPs (**Figure 3C**). Quantitative analysis (**Figure 3D**) showed there was enhanced accumulation of curcumin in the brain after 6 h, which peaked after 24 h.

In vivo permeability and pathology evaluation of CPC with UTMD

Next, we investigated the potential of employing CPC with UTMD to locally open the BBB around the targeted brain nuclei, the corpus striatum. Healthy C57BL/6 mice were randomly divided into five groups: (1) control; (2) only curcumin-loaded cerasomes with no PS 80; (3) only CPC with 5% PS 80; (4) 5% PS 80-modified cerasomes with no curcumin in combination with UTMD; (5) CPC with 5% PS 80 in combination with UTMD. The focused ultrasound system (FUS) equipped with a cyclic transducer was applied, and the physical ultrasound focus was positioned on the left corpus striatum of C57BL/6 mice (**Figure 4A-B**). After i.v. administration of MBs with mean diameters of 1.259 μm (**Figure S1**) and CPC NPs, BBB opening was induced by ultrasound, and the efficacy of targeted curcumin permeability was evaluated via fluorescence imaging of ex vivo brains. As shown in **Figure 4C-D**, similar to control group 1, there was almost no fluorescence signal in group 2 treated by the curcumin cerasomes with no PS 80 and no UTMD, or in group 4 treated by the 5%

PS 80-modified cerasomes with no curcumin in combination with UTMD. In sharp contrast to group 2, the CPC NPs-treated group 3 showed apparent fluorescence, indicating that the PS 80 surface modification boosted the delivery of the curcumin-loaded cerasomes into the brain of animals. In combination with UTMD, the CPC NPs-treated group 5 exhibited 3.31-, 1.62-, 1.59- and 1.31-fold higher curcumin fluorescence signal than group 3 at 0.1 h, 6 h, 12 h and 24 h, respectively. Interestingly for group 5, the left corpus striatum showed 1.7-fold higher curcumin accumulation than the right corpus striatum 6 h after administration of CPC NPs and MBs. The fluorescence signal intensities increased with time and reached a peak at 24 h.

Hematoxylin and eosin (H&E) histopathology images (**Figure 4E**) revealed no evidence of acute or chronic inflammation, necrosis, microvascular changes or microhemorrhages in the CPC-UTMD group one week after the administration compared with the group treated with normal saline. Together, these findings suggested that the system is a safe and effective way of delivering curcumin for in vivo experiments.

Uptake and protective property of CPC in a MPP+-induced PD cell model

Human neuroblastoma cells (SH-SY5Y) were induced by MPP+ (1-methyl-4-phenylpyridine) for to generate a PD model and an in vitro BBB model was developed by seeding a monolayer of brain microvascular endothelial cells (B.End.3) onto a transwell membrane. As displayed in **Figure 5A**, UTMD was applied on the B.End.3 layer of the BBB cell model to prove the safety of the CPC-UTMD delivery system, and the B.end.3 cell viability was evaluated (**Figure S2B**). Neither the CPC NPs nor UTMD involved in these 5 groups appeared to be toxic to B.end.3 cells after a 24 h incubation period, because the viability rates were all around 100%. From confocal laser scanning microscopy (CLSM) experiments to measure permeation, there was evidence that the UTMD downregulated the expression of the tight junction protein, zonula occludens-1 (ZO-1), in groups 4 and 5, but no alteration in the other groups was observed (**Figure S2B**). As an intracellular protein network, ZO-1 plays a role in forming tight junctions by anchoring transmembrane proteins. When ZO-1 levels decrease, the intercellular connections are not strong enough to inhibit paracellular transport. The results indicated that the cells applied with UTMD maintained intact organization but permeable membrane compared to the untreated B.end.3 cells. In summary, the system of CPC-UTMD was non-toxic and efficient for curcumin delivery.
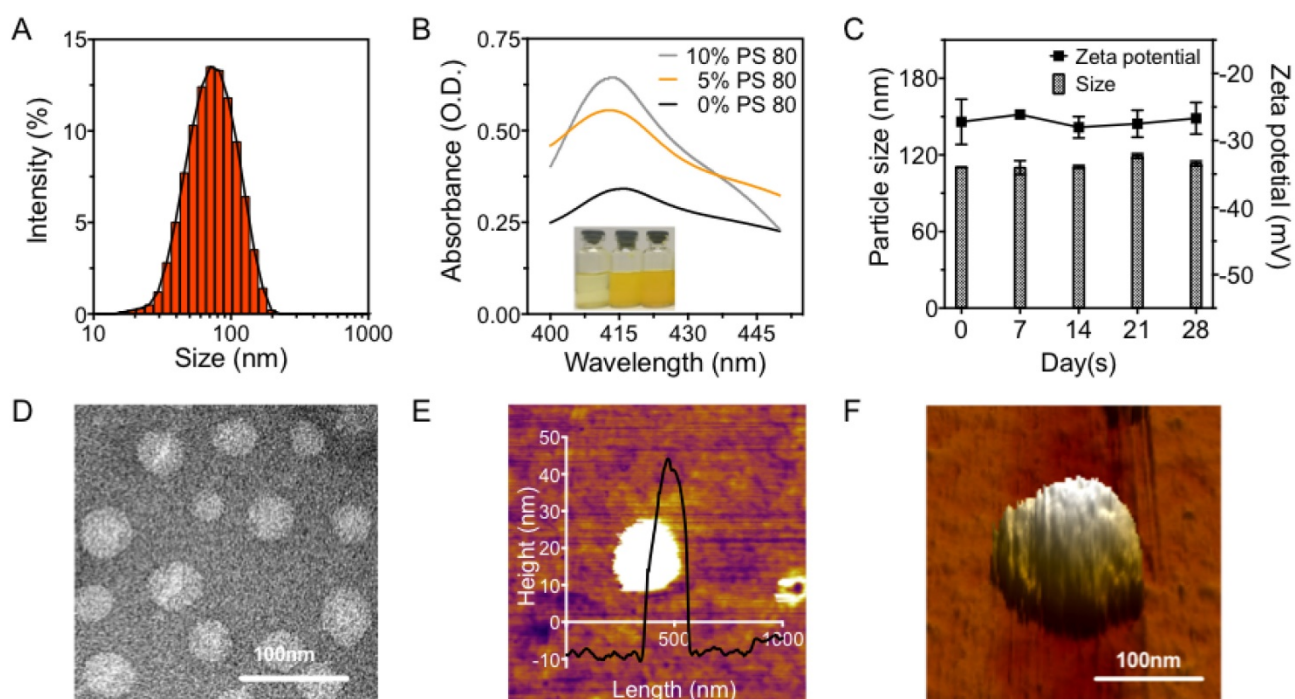
Figure 2. Characterization of CPC NPs. (A) The CPC particle size distribution as measured by DLS. **(B)** The UV-Vis absorption spectra and appearance of the CPC NPs with different weight ratios of PS 80. **(C)** The zeta potential and size changes of CPC NPs with 5% of PS 80 measured within a month. **(D)** The TEM image of CPC with 5% of PS 80. The representative 2D **(E)** and 3D **(F)** AFM images revealed that the CPC NPs with 5% of PS 80 maintained a spherical shape.
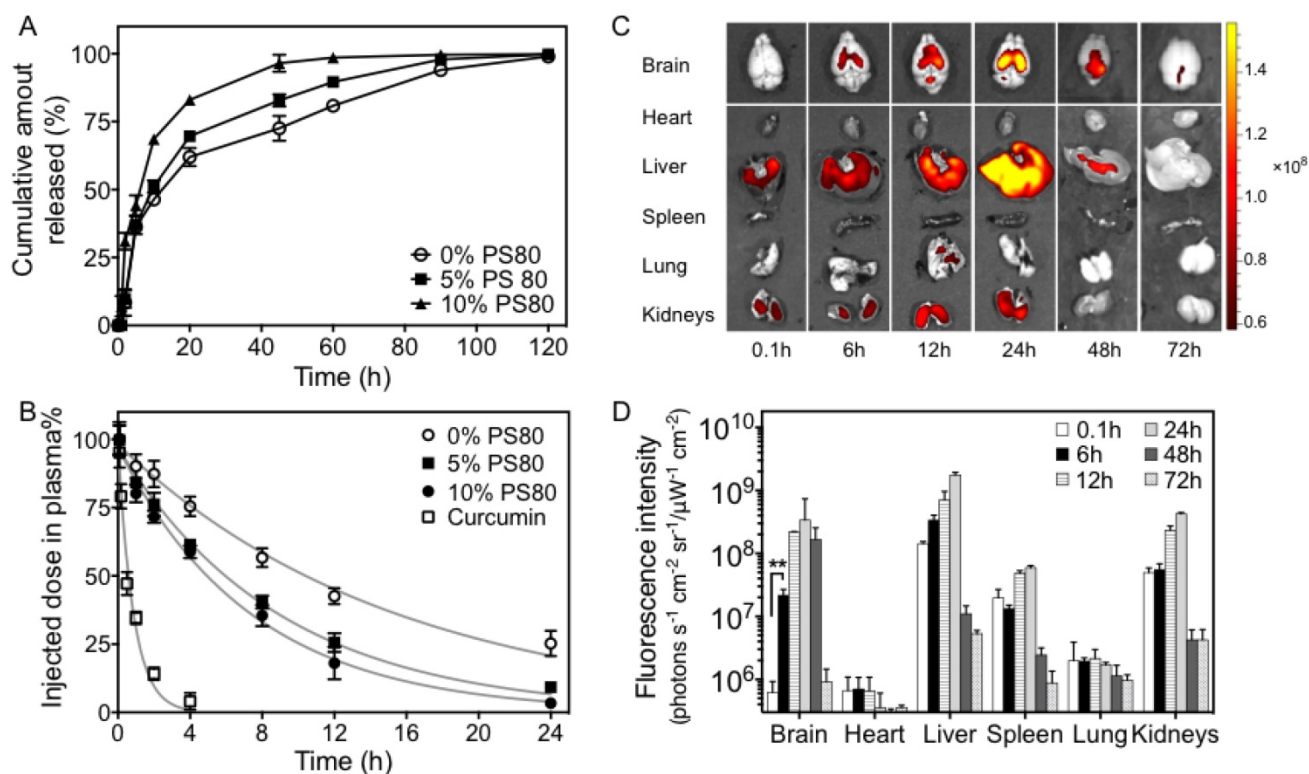

Figure 3. The releasing behavior in vitro, pharmacokinetic profile and bio-distribution in vivo of CPC NPs. (A) The releasing behavior in vitro and **(B)** the pharmacokinetic profiles of the curcumin level in blood plasma from CPC NPs with 0% to 10% of PS 80 (n=6 per group). **(C)** The fluorescence images and **(D)** the quantitative graph of the fluorescence intensity of curcumin in the major organs collected at 0.1, 6, 12 and 24 h after CPC intravenous (i.v.) administration combined with UTMD (n=6 at each time point). Significance is marked as ** P<0.01.
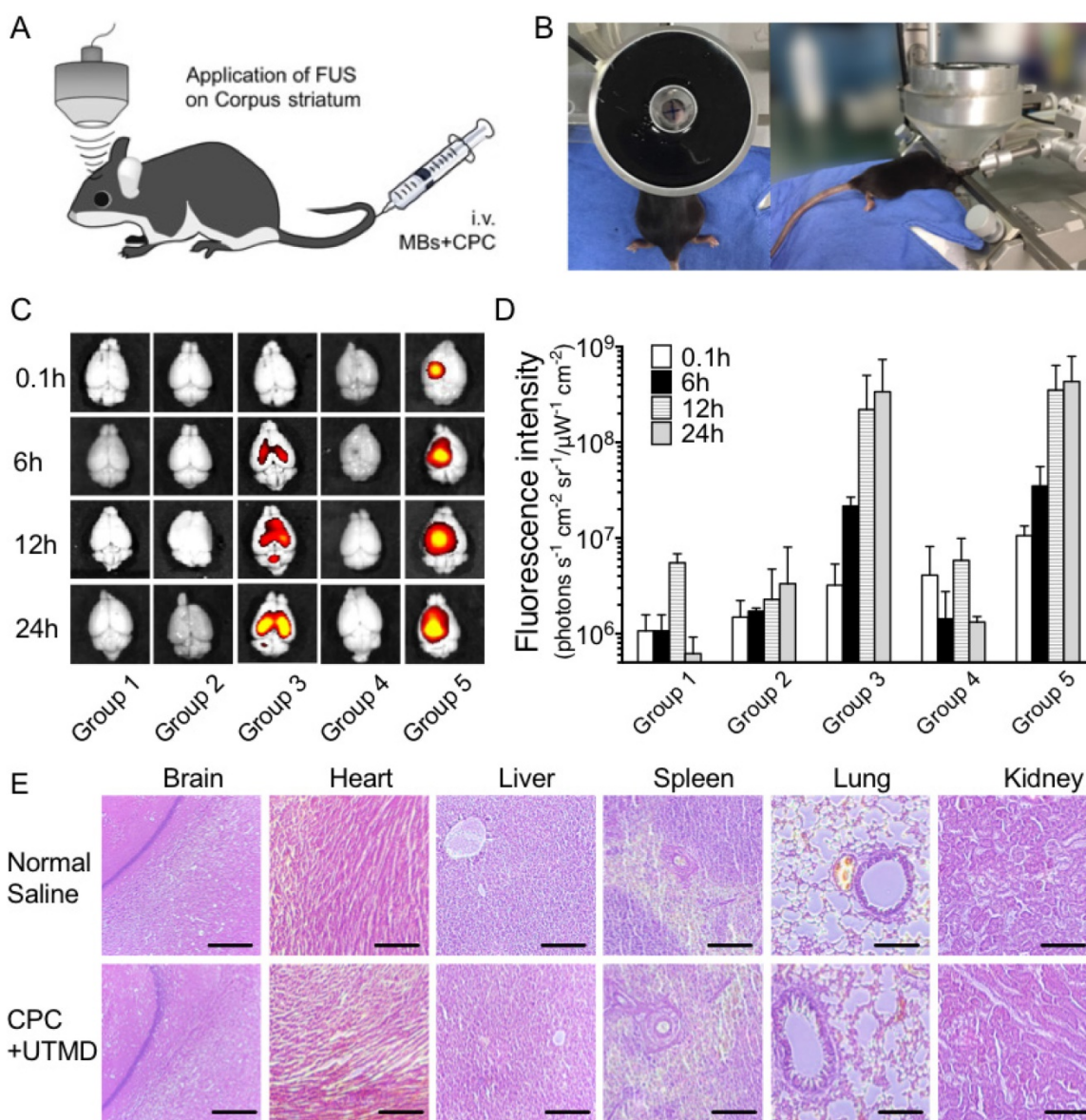
Figure 4. The permeability and pathology evaluation of CPC with 5% PS80. (A) Schematic and **(B)** photograph of the UTMD setup for local treatment of the corpus striatum of C57BL/6 mice. **(C)** The representative ex vivo fluorescence images and **(D)** the measurement of the radiance counts of fluorescence intensity by IVIS imaging software at 0.1, 6, 12 and 24 h after i.v. administration (n=6 per group at each time point). **(E)** H&E staining for histopathological evaluation of major organs in the group treated with normal saline and with CPC-UTMD (n=6 per group). Scale bars represent 50 μm.

The neuronal internalization of the CPC NPs was observed by CLSM and quantified by fluorescence spectrometry in dopaminergic SH-SY5Y cells. **Figure 5B** shows that the CPC NPs definitely localized in the nuclei, demonstrating that CPC NPs could penetrate through the B.end.3 cell layer and enter SHSY-5Y cells after the UTMD treatment and 4 h incubation. As shown in **Figure 5C**, no curcumin fluorescence was detected in groups 1 and 4, while curcumin fluorescence was found to increase with incubation time in groups 2, 3 and 5. Throughout the incubation time, the curcumin fluorescence intensity elevation was of the order: group 2 < group 3 < group 5. This demonstrated that both the PS 80 surface modification

and the employment of UTMD could result in an enhanced cellular uptake of CPC NPs.

In addition, after 24 h treatment, SH-SY5Y expressed the dopaminergic markers for dopamine synthesis, tyrosine hydroxylase (TH), and more importantly, the western blotting results verified the re-enhancement of TH to the normal level in groups 3 and 5 but not in group 2. At the same time, the quantified AS level also ascertained that curcumin played a critical role in removing the aggregated AS, especially in group 5, which delivered curcumin with PS 80-modified cerasomes as well as UTMD application (**Figure S3**).
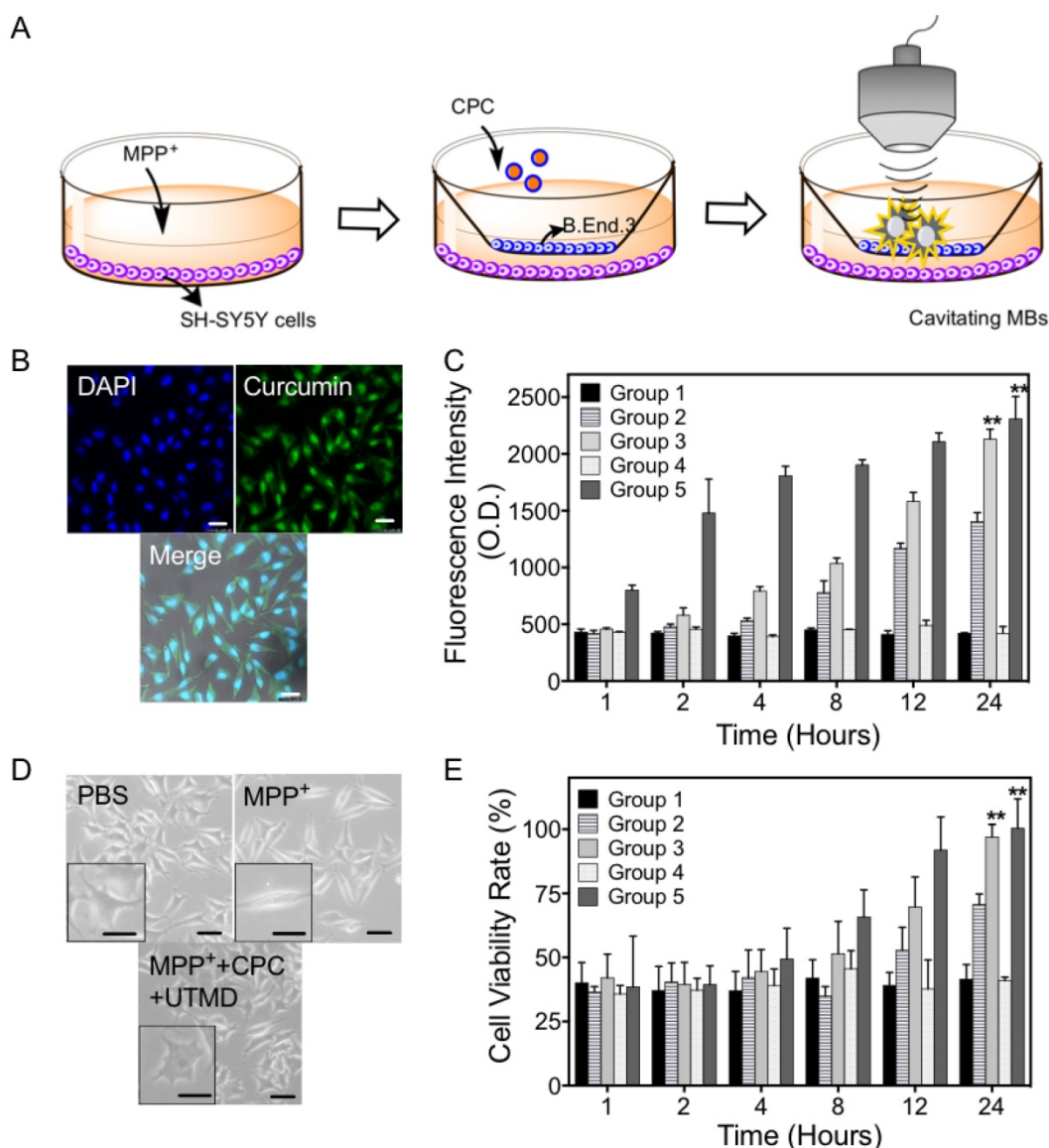
Figure 5. The uptake and protective property of CPC NPs in vitro. (A) The schematic of the process for both BBB and PD in vitro cell model establishment. Fluorescence of curcumin cellular uptake tested by **(B)** the CLSM observation and **(C)** the spectroscopic measurement of different treatment groups over time. The comparison of **(D)** the morphological change and **(E)** the cell viability rate by CCK-8 assay in SH-SY5Y with different treatments during continual observation to reflect the protective property of CPC in the PD cell model. Significances are marked as * P<0.05 and ** P<0.01 vs. MPTP group. Scale bars represent 10 μm.

From observation of cellular morphology, after MPP+ treatment, PD-like cells possessed a number of vacuoles inside the cell and these cells appeared a little longer with fewer synapses. However, after 12 h incubation and CPC NPs uptake, these morphologic changes were compromised (**Figure 5D**), which suggested that CPC NPs indeed helped the PD-like cells to recover from the morphological alterations and necrosis. Consistent with the results from the cell viability test, CPC NPs showed a protective effect on the MPP+-treated cells. The phenomenon was particularly obvious at 12 h, as the viability rate of group 5 rose to 91.9%, while those of groups 2 and 3 were only 52.8% and 69.7%. After 24 h incubation, 97.7% and 100.4% of cells were greatly recovered in groups 3 and 5, whereas only 70.7% of cells still survived in group 2. Compared with the normal SH-SY5Y cells, the viability ratios of the PD-model group and the group treated with blank cerasomes and UTMD were ~40% after 24 h incubation.

The motor behavior and striatum dopamine content of C57BL/6 mice

The therapeutic effect for PD progression control was assessed. Behaviors reflecting the recovery status of PD mice were observed and recorded. A decline in grip strength and increased latency in akinesia and catalepsy are the indications of reduced motor activities. Both the recorded elapsed time in the rotary-rod test and the run duration time in the climbing-pole test reflected the motor asymmetry recovery status of the C57BL/6 mice, which were

divided into 6 groups (**Figure 6A-B**). Similar to group 1 treated with MPTP and observed for two weeks, a loss of significant motor activities was seen in groups 2 and 4, which were treated with curcumin-loaded cerasomes and blank cerasomes with UTMD, respectively. For the PD model mice, the time sustained on the rotatory rod was 58-80 s, and the run duration on the climbing pole was 11-14 s, while the healthy mice presented balanced and normal motor function. Additionally, an obvious difference was observed between groups 3 and 5. Group 3 did not gradually recover until the four treatments with CPC NPs. Notably, group 5 rapidly produced PD-like syndrome alleviation and eventually reached a fully normal level after four treatments with CPC-UTMD. The elapsed time on the rotatory rod was recovered

from ~60 s to >200 s, and the run duration time on the climbing pole decreased to <5 s.

Correspondingly, the observed appearance of Parkinsonian motor symptoms in the mice was importantly linked with the loss of striatal dopamine (DA). The DA level was measured by high-performance liquid chromatography with electro-chemical detector (HPLC-ECD). As shown in **Figure 6C-D**, compared with the controls, the mean contents of DA and its metabolites DOPAC and HVA in the striatum were significantly depleted in groups 1 and 4, suggesting severe dopaminergic neuron loss caused by MPTP. Groups 2 and 3 had partly restored DA and its metabolites after 2 weeks, while there was abundant DA and its metabolites in group 5.
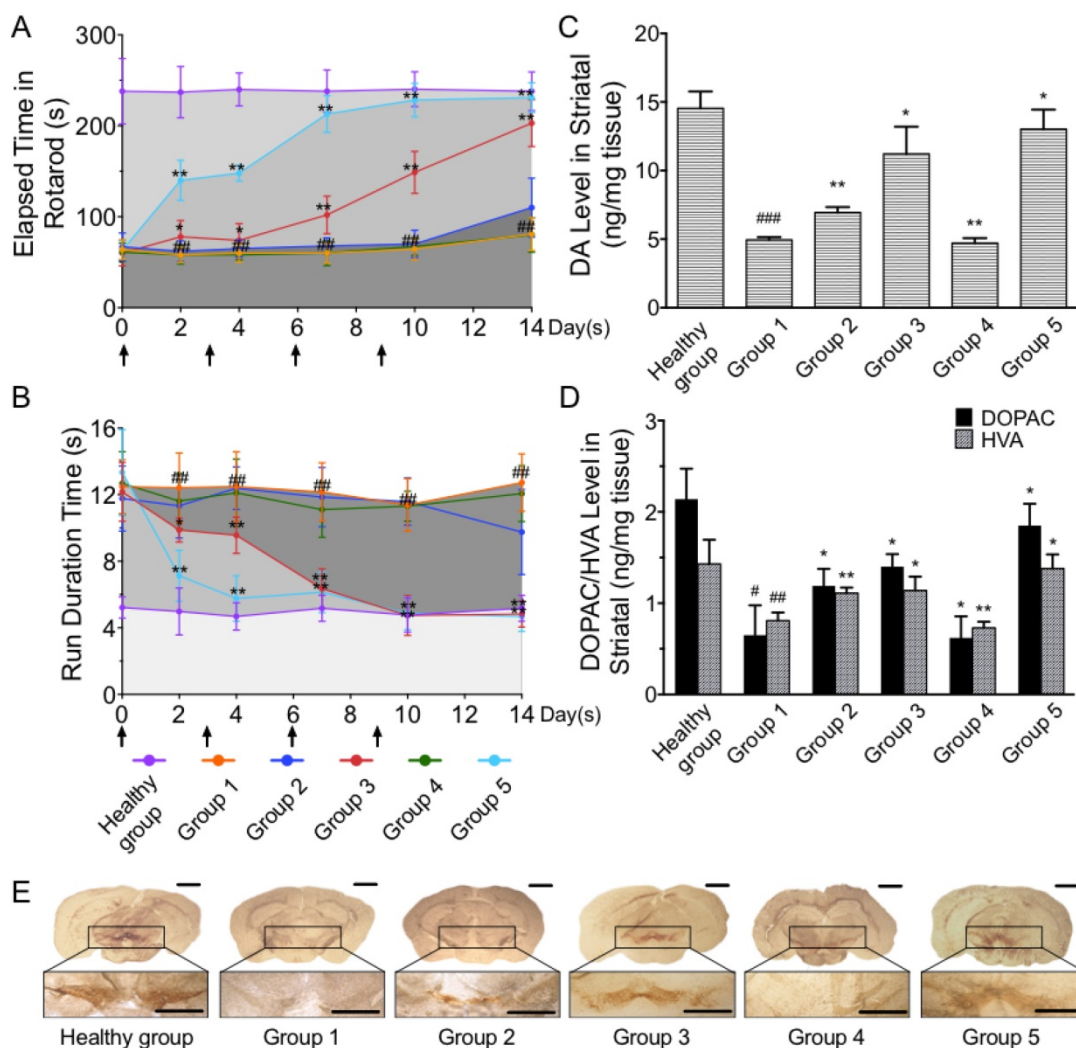

Figure 6. The motor behavior and expression levels of C57BL/6 mice reflecting their MPTP-induced PD level. (A) Rotatory-rod test and **(B)** climbing-pole test were carried out over a period of 2 weeks for the evaluation of PD severity following injection of CPC NPs 4 times at 0, 3, 6 and 9 days after the construction of the MPTP-induced model (n=10 per group). The levels of **(C)** DA and **(D)** DOPAC and HVA in striatum of C57BL/6 mice in each group, which reflected the rehabilitative situation of the mice (n=10 per group). **(E)** The representative IHC staining pictures of TH at SN in the mouse brain sections for different groups (n=6 per group). Significances were marked as # $P<0.05$ vs. control group, ### $P<0.001$ vs. control group, * $P<0.05$ vs. MPTP group and ** $P<0.01$ vs. MPTP group. Scale bars represent 2 mm.

Likewise, the dopaminergic neuron recovery efficiency in SNC after curcumin delivery was histologically confirmed. The brain sections for each group were stained via immunohistochemistry (IHC) of TH to observe the dopaminergic structures in SNC for potent neuroprotective and neurotrophic assessment (**Figure 6**E). TH absence was observed at the MPTP effect site in groups 1, 2 and 4, indicating the severe pathogenesis of PD. Yet, groups 3 and 5 showed successfully recovered dopaminergic neurons by dense TH stains at the SNC.

Discussion

A curcumin-loaded polysorbate 80-modified cerasome was successfully developed by addition of PS 80 to the lipid-curcumin thin film using a thin-film hydration method to overcome the problems associated with the delivery of curcumin across the BBB for improved PD treatment in combination with ultrasound-targeted microbubble destruction. The liposomal nanohybrid cerasome exhibited superior stability towards PS 80 surfactant solubilization, which was attributed to siloxane networks with certain densities that blocked the drug release channels. The CPC NPs with 5% PS 80 showed a long circulation lifetime ($t_{1/2}$ = 6.22 h), much longer than free curcumin ($t_{1/2}$ = 0.76 h). In addition, the PS 80 surface modification was found to remarkably enhance the penetration of curcumin-loaded cerasomes across the BBB by transcytosis through vascular endothelial cells, and with the additional use of UTMD, BBB opening was induced to allow extravasation of CPC NPs into the brain from the systemic circulation, resulting in an increased uptake of curcumin in the UTMD-treated brain side.

MPTP-induced neuronal degeneration was associated with systemic complex I defect, and the redistribution of AS from its normal synaptic location to aggregates in degenerating neuronal cell bodies [54, 55]. AS aggregation resulted from MPTP can model the early stages of Lewy body formation and is fundamental in the evolution of neuronal degeneration in PD [56]. The chronic MPTP model exhibits numerous PD pathological and physical features [57], and leads to the accumulation and nitration of AS in the cytosol of SNpc dopaminergic neurons [58, 59]. Thus, the MPTP-induced PD model was chosen for further exploration of the CPC NPs' therapeutic effect.

All the evidence in the in vitro cell experiment proved the protective effect on the MPP+-induced PD cells model and the permeability of curcumin through the BBB model layer owing to the help of UTMD and PS 80 modification for the cerasomal carriers. This study also solved the key problem in PD treatment and optimized the approach parameters for curcumin delivery. These feasibility studies were to help curcumin pass through the BBB and reach the striatum to exert effects on the recovery of a MPTP-induced PD mouse model by downregulating the aggregation of misfolded protein, AS. After intravenous administration of CPC NPs followed by synergic UTMD application to induce BBB opening regionally and noninvasively, the localized delivery of the CPC NPs into mouse brain nuclei was achieved. We observed high competency in AS clearance in vitro and optimal neuroprotection effects in MPTP-induced PD mice.

Notably, changes in motor behaviors revealed that the employment of UTMD could accelerate the CPC NPs delivery into the brain for behavior recovery in PD mouse models. Additionally, DA level and TH expression all returned to normal. This result demonstrated rehabilitation from AS aggregation in the process of neurodegeneration. It is also important to highlight that the murine models used in routine experiments can barely mimic the real environment of PD or other similar neural disorders. However, alternative methodologies encompassing complex neural networks such as rhesus models could be used as a next step to confirm the efficacy of CPC-UTMD.

The high physiological stability of CPC NPs is beneficial to avoid premature drug release in plasma, and UTMD application guarantees the drug accumulation to targeted brain nuclei for successful PD rehabilitation, reducing certain undesirable complications. In recent years, Lin C Y et al. designed glial cell line-derived neurotrophic factor (GDNF) gene-loaded liposomes with the UTMD technique to treat MPTP-induced PD mice at the SN site, which proved that the delivery system was successful and efficient [60]. There are also many other strategies that have been attempted to use CNS gene-loaded microbubbles for brain disease therapy [35, 61-63]. Compared with these studies, the CPC-UTMD has overwhelming advantages not only for its relatively high drug-loading capacity and long blood circulating stability, but also for efficacious chemotherapy avoiding gene off-target side effects. In the future, this paradigm will be extended to design extensive therapeutic agents in other neurodegenerative models, and consequently improve clinical proced-ures and therapeutic outcomes for PD treatment.

Materials and methods

Lipids and chemical reagents

All chemicals and lipids were commercially available and used as obtained. Cerasome-forming lipid (CFL), N-[N-(3-triethoxysilyl)propylsuccinam-

oyl]-di-hexadecylamine, was synthesized according to the reported method [47, 50]. Curcumin was purchased from Sigma Aldrich (Steinheim, Germany). The organic solvents, chloroform, and polysorbate 80 were purchased from Sinopharm Chemical Reagent, China. Distearoyl phosphatidylcholine (DSPC) and 1,2-distearoyl-sn-glycero-3-phosphoethanolamine-N-[maleimide(polyethylene glycol)-2000] (DSPE-PEG 2000; Lipoid, Ludwigshafen, Germany) were used for microbubble synthesis according to the reported method [31, 64]. Dulbecco's modified Eagle's medium (DMEM), fetal bovine serum, penicillin, and strepto-mycin were all purchased from Thermo Fisher Scientific, USA. All other reagents were of analytical grade. The C57BL/6 mice, weighing about 20 g (6 weeks old), were obtained from Guangdong Medical Experimental Animal Center (Guangzhou, China). All the animal experiments were approved by the Institutional Animal Care and Use Committee (IACUC) and carried out ethically and humanely.

Preparation of CPC NPs

The curcumin-loaded cerasomes were coated with PS 80 at different compositions. CPC was prepared from CFL using a thin-film hydration method in combination with sol-gel reaction and self-assembly process. The organic solvent, chloroform, was entirely removed from the mixture of CFL and curcumin by vacuum rotary evaporation (90 rpm, 55 °C; Rotavapor R-210, Switzerland), until a thin dried lipid film was formed. PS 80 at 0%, 5% or 10% of the lipid in ultrapure water was added to the film and hydrated at 55 °C. Upon ultrasonication (SB120 DT, NingBo Scientz Biotechnology, China), the liposomal bilayer self-assembled and rigidified via in situ sol-gel reaction on the surface overnight. The particles were ultrasonically dispersed for a while, and the free curcumin was removed by centrifugation (4800 rcf, 10 min, 4 °C) [47, 50].

Characterization of CPC NPs

The average diameter, zeta potential and size distribution of PS 80-coated curcumin-loaded cerasomes were determined by dynamic light scattering (DLS; Zetasizer Nano ZS, Malvern Instrument, UK) [44, 45], and the DLS was measured every other day for a month to test the stability of the particles. The morphologic examination was further performed by AFM (MPF-3D-BIO, Oxford Instruments Asylum Research, USA) and TEM (Tecnai G2 F20 S-Twin, FEI, USA) [31]. Before analysis, the test samples for AFM observation were placed on a clean and smooth glass slide and air-dried for a while, and the samples were placed on a carbon-coated copper grid, and negatively stained with 2% (w/v) phosphotungstic acid and air-dried prior to TEM observation. The encapsulation efficiencies (EE) and drug loading capacity (DLC) of curcumin in all the formulations were determined. Firstly, a calibration curve was set with curcumin at concentrations of 0, 10, 20, 50, 100, 200, 500, 1000 mg/L analyzed using a UV-Vis spectrophotometer (Lambda25, PerkinElmer, USA) at the wavelength of 414 nm. The CPC samples were diluted and analyzed in the same way. The concentration of curcumin was calculated according to the calibration curve. The formula of EE and DLC are [50]:

$$EE\ (\%) = Conc._{\text{curcumin contained}} / (m_{\text{curcurmin added}} / V_{\text{sample}}) \times 100$$

$$DLC\ (\%) = Conc._{\text{curcumin contained}} / (m_{\text{PS 80 and CFL}} / V_{\text{sample}}) \times 100$$

Effect of vesicular composition on the release behavior: 2 mL curcumin-cerasome sample was added to a dialysis tube (MW 8000-14000, Solarbio, China) and the tube was rotated in a beaker with 200 mL of PBS at a temperature of 37 °C. After 1, 2, 5, 10, 20, 45, 60, 90 and 120 h, 1 mL of solution was taken out to analyze the concentration by UV spectroscopy and 1 mL of PBS was replenished. The cumulative amount of drug released in contrast to the original drug contained was calculated according to the formula [50]:

$$\text{Cumulative amount released}\ (\%) = Conc._{\text{drug released}} / conc._{\text{drug contained}} \times 100$$

Pharmacokinetic profiles of CPC

The blood pharmacokinetics of CPC in different ratios were monitored in healthy C57BL/6 mice. Blood samples (at least 100 μL) were withdrawn from the retro-orbital sinus and collected into heparinized microcentrifuge tubes (containing 20 mL of 1000 IU heparin/mL of blood) at 0.1, 0.5, 1, 2, 4, 8, 12, 24 h after intravenous (i.v.) injection of CPC (15 mg curcumin/kg) (n=6 per group at each time point). After each sampling, 100 μL of dextrose–normal saline was administered to prevent changes in the central compartment volume and electrolytes. The pharmacokinetics profile of CPC in the bloodstream was finally evaluated by measuring the curcumin content in blood over the course of 24 h via fluorescence spectrophotometry measurement (LS-55, PerkinElmer, USA; ex. = 420 nm, em. = 450 nm) after decomposing the blood samples by aqua regia. The curcumin content in the plasma was measured according to reported methods [39]. Briefly, the plasma was separated by centrifuging the blood samples (4000 rcf for 10 min, 4 °C) and stored at -20 °C until analysis. The supernatant was transferred into a 96-well plate for determination of fluorescence at the

excitation wavelength of 414 nm and the emission wavelength of 450 nm. The percentage of the injected dose in the blood (ID%/g) over time, the area under the plasma concentration-time curve (AUC), and the half-life time ($t_{1/2}$) were calculated. The results were evaluated using the Kinetica software package (version 5.0, Thermo Fisher Scientific, USA) [50]:

$$ID \% / g = (C_t / C_{injected}) / W_{body} \times 100$$

$$AUC_{0 \to \infty} = AUC_{0 \to t} + C_t / K_e$$

Where C_t is the curcumin concentration observed at the last time, and K_e is the apparent elimination rate constant obtained from the terminal slope of the individual plasma concentration–time curves after logarithmic transformation of the plasma concentration values and application of linear regression. Systemic elimination or clearance of curcumin from the body is also an important factor, which determines its relative biological activity:

$$t_{1/2} = 0.693 / k_1$$

$$k_1 = 2.303 \times (\log C_1 - \log C_2) / (t_1 - t_2)$$

Here, k_1 is the first-order kinetic constant, and C_1 and C_2 are the curcumin concentrations in blood plasma at times t_1 and t_2, respectively [50].

Biodistribution study of CPC NPs

Uptake and distribution of curcumin in body tissues is crucial for its biological activity. The biodistribution of the curcumin-loaded cerasomes was studied in mice, which were divided into groups: (1) control; (2) only curcumin-loaded cerasomes with no PS 80; (3) only CPC with 5% PS 80; (4) 5% PS 80-modified cerasomes with no curcumin in combination with UTMD; (5) CPC with 5% PS 80 in combination with UTMD (group 5 was treated only on the left side for distinction from group 3). The anesthetized mice (n=6 per group at each time point) were transcardially perfusion-fixed with 4% polyformaldehyde (PFA) in PBS. The curcumin content in dissected major organs (brain, heart, liver, spleen, lung and kidney) ex vivo was measured using the IVIS imaging system (Caliper IVIS Spectrum, PerkinElmer) on the basis of the fluorescence intensity from curcumin (ex. = 420 nm, em. = 520 nm), at 0.1, 6, 12, 24 h after i.v. [50].

Construction of in vitro BBB model and MPP+-induced PD cell model

Brain microvascular endothelial cells (B.End.3) were suspended in plating medium (RPMI 1640 (Gibco, USA) and seeded on rat-tail collagen-coated polycarbonate membranes (transwell permeable support, 24-well plate) at a density of 250,000 cells/cm^2 [20]. After the cells had reached confluence (in general after 48 h), the trans epithellal electric resistance (TEER) value of the cells was measured by CellZScope (NanoAnalytics, Germany) above 700 Ω/cm^2 (the TEER values were measured during the 48 h incubation). The eligible cell layers were screened as in vitro BBB models for the transfer experiments. MPP+, the active metabolite of MPTP, was used to cause damage to the SH-SY5Y cells for constructing a PD cell model [9]. SH-SY5Y were seeded in 24-well plates and 1 mM MPP+ was added and treated for 36 h, with PBS of the same amount for the control group. After the SH-SY5Y cells were morphologically changed, B.End.3-seeded transwells were placed over them. 5 groups for the experiment were introduced into the apical side chamber (blood side in vivo) of the BBB model: (1) PBS-treated only as a model group; (2) curcumin cerasomes; (3) CPC; (4) cerasomes in combination with UTMD; (5) CPC-UTMD.

Fluorescence observation and measurement of the cell uptake of curcumin

0.1, 4, 8, 12, 24 and 48 h after treatment, the basolateral SH-SY5Y cells were collected into EP tubes by centrifugation (200 rcf for 4 min at 4 °C), washed with PBS, and fixed by 4% cold PFA for 10 min at 4 °C. The fixed cells were washed and resuspended in PBS. To compare the permeability of curcumin through the B.End.3-established BBB model, the curcurmin fluorescence per 10,000 cells was measured by fluorescence spectrophotometry. After 48-h CPC treatment, the fluorescence uptake was observed upon CLSM (Leica TCS SP5, Germany; ex. = 420 nm, em. = 450 nm). The cells were washed with PBS and fixed by PFA for 10 min, and then washed in the same way. The cell nuclei were stained with DAPI (ex. = 340 nm, em. = 488 nm) to localize the cells.

Cell viability evaluation

The basolateral cells in medium were collected and the cell viability was analyzed by CCK-8 assay (cell counting assay) at 0.1, 6, 12, 24 and 48 h after MPP+ exposure and with experimental treatments. The absorbance was calculated by Multiskan at the wavelength of 465 nm and the viability rate was calculated according to the formula:

$$\text{Cell viability rate } (\%) = A_{465, sample} / (A_{465, contrast} - A_{465, blank}) \times 100$$

The cell viability in different groups was compared with statistic process of t-test [50].

Cellular morphological changes

The transwells with B.End.3-established BBB model were removed, and the treated SH-SY5Y cells were placed under the microscope for observation of

morphological changes to compare the living state of the cells.

Construction of MPTP-induced PD mouse model

Based on the intact BBB, MPTP-induced PD mouse model was chosen for all experiments. The C57BL/6 mice were treated by repeated intraperitoneal injections (i.p.) of MPTP (40 mg/kg) solution for 7 days consecutively. The mice were randomly divided into 5 groups [5, 13]: (1) control; (2) only curcumin-loaded cerasomes with no PS 80; (3) Only CPC with 5% PS 80; (4) 5% PS 80 modified cerasomes with no curcumin in combination with UTMD; (5) CPC with 5% PS 80 in combination with UTMD (15 mg/kg curcumin was administered with 2×10^8 MBs/kg). The mice were treated every two days for four times to ensure effective drug accumulation in the brain. For the groups with UTMD application, the mice were depilated under 10% chloral hydrate anesthesia (10 g/100 mL normal saline, 4 mL/kg i.p.), and were then mounted onto a stereotactic frame. The focus point of the ultrasonic probe was firstly set at the bregma as the original point and then adjusted precisely to the corpus striatum in medial forebrain bundle (MFB), referred to as the brain atlas. The focused ultrasound beam was generated by a single-element spherical transducer (center frequency: 1.2819 MHz; focal length: 51.3 mm; cycle: 10.000 k), a function generator (AFG3102C, Tektronix, Beaverton, USA), and was driven by a 50 dB power amplifier (325LA, Electronics & Innovation, Rochester, USA) according to the reported research [64]. The ultrasound was performed for 60 s on both sides of the brain after different administrations i.v.

Behavioral tests

In the rotary rod test to observe fatigue and grip strength of mice, the elapsed time that each mouse walks on the rotatory rod at a speed of 25 rpm was recorded at least 3 times after training once. In the climbing pole test to observe the behavior disorder situation, the run duration time that mice climb from the top of the 60 cm long pole to the bottom was recorded at least 3 times after training once. The behavioral tests reflected the recovery status of the C57BL/6 mice with different treatments (n=10 per group) [57, 58].

Determination of dopamine level

After 2-week observation, the mice were sacrificed and the paired striatal tissues (n=10 per group) were separated, weighed and then homogenized in 250 μL ice-cold 0.3% perchloric acid using a homogenizer. The suspension was centrifugated (4 °C, 10000 rcf, 10 min), and the supernatant was collected and filtered through a 0.2 μm filter membrane. The processed samples were lyophilized at a temperature of -22 °C and re-suspended by 40 μL of ice-cold 0.3% perchloric. The mobile phase was prepared: 20.2 g of trisodium citrate, 0.036 g of EDTA, 13.64 g citric acid and 100 mL methanol were mixed and diluted with ultrapure water to a constant volume of 1 L; the solution was filtered by a 0.22 μM filter membrane and degassed. The calibration curve was prepared with a standard solution at concentrations of 50, 200, 500, 1000, 2000 and 5000 μg/L by HPLC-ECD (Model 5600A, ESA, USA) with a reverse phase C18 column (ZORBAX Eclipse XDB, Agilent, USA; column temperature: 25 °C, flow rate: 0.8 mL/min, cell temperature: 4 °C). The absorbance from sample analysis was analyzed to deduce the concentration of DA and its metabolites (DOPAC and HVA), and their amount in the striatal tissues was calculated [58, 65].

TH immunohistochemistry (IHC)

The restoration of DA neurons in mice was confirmed by TH IHC staining. 2 weeks after the different treatments, the brains of mice (n=6 per group) were acquired and post-fixed. The serial coronal frozen sections of the brain (20 μm thickness) were obtained and incubated overnight with a monoclonal mouse TH primary antibody (Abcam, 1:200 dilution). After rinsing in tris-buffered saline with tween (TBST), the sections were incubated with secondary goat anti-rabbit IgG-horseradish peroxidase (HRP) antibody (Abcam, 1:200 dilution) for 1 h at room temperature. The activity of HRP was presented by diaminobenzidine (DAB) substrate. The microscope images of SNC were read as gray levels and integrated [35].

Histopathology evaluation of CPC in vivo

A subset of mice were tested to determine whether CPC was toxic by observation and histopathological evaluation. The mice injected with CPC NPs (n=6 per group) survived for one week, as long as we followed them, without any overt signs of physical distress and injury. The histopathology of major organs (brain, heart, liver, spleen, lung and kidneys) was evaluated by hematoxylin and eosin (H&E) staining.

Statistical data analysis

For all the experiments, the data was analyzed as the mean ± standard deviation (STDEV) using Microsoft Excel 2016. The tests for significant differences between the groups were performed using a Tukey test (t-test) or one-way ANOVA with multiple comparisons using SPSS 23.0 and GraphPad

Prism 7.0 (p<0.05 means the results were statistically significant).

Supplementary Material

Supplementary methods and figures.
http://www.thno.org/v08p2264s1.pdf
Supplementary Movie 1.
http://www.thno.org/v08p2264s2.mp4
Supplementary Movie 2.
http://www.thno.org/v08p2264s3.mp4

Acknowledgements

Author Contributions

N. Z. designed and performed the experimental work, analyzed the data and wrote the manuscript. F. Y. proposed the hypothesis, modified the experimental procedures, approved the data analysis, and revised the manuscript. X. L., Y. X. and G. Z. conducted the synthesis of CFL and supporting techniques. M. W. conducted the in vivo imaging experiments and H&E staining analysis. Y. S. provided the ultrasound equipment for UTMD operation. C. T. conducted the synthesis and characterization of microbubbles. M. C. optimized the modification of the experimental procedures. P. J. conducted the AFM application on the characterization of CPC nanoparticles.

Competing Interests

The authors have declared that no competing interest exists.

References

1. Lang A E, Lozano A M. Parkinson's Disease. Lancet. 1998; 386: 896-912.
2. Lees A J. The relevance of the Lewy Body to the pathogenesis of idiopathic Parkinson's disease: accuracy of clinical diagnosis of idiopathic Parkinson's disease. J Neuro Neurosurg. 2012; 83: 954-5.
3. Schapira A H. Neurobiology and treatment of Parkinson's disease. Trends Pharmaco Sci. 2009; 30: 41-7.
4. Pezzoli G, Zini M. Levodopa in Parkinson's disease: from the past to the future. Expert Opin Pharmacother. 2010; 11: 627-35.
5. Hammond C, Bergman H, Brown P. Pathological synchronization in Parkinson's disease: networks, models and treatments. Trends Neurosci. 2007; 30: 357-64.
6. Ray C K, Rojo J M, Schapira A H, et al. A proposal for a comprehensive grading of Parkinson's disease severity combining motor and non-motor assessments: meeting an unmet need. Plos One. 2013; 8: e57221.
7. Cacabelos R. Parkinson's Disease: From Pathogenesis to Pharmacogenomics. Int J Mol Sci. 2017; 18: 551.
8. Kalinderi K, Bostantjopoulou S, Fidani L. The genetic background of Parkinson's disease: current progress and future prospects. Acta Neuro Scand. 2016; 134: 314-26.
9. Jackson-Lewis V, Przedborski S. Protocol for the MPTP mouse model of Parkinson's disease. Nat Protoc. 2007; 2: 141-51.
10. Martínez-Fernández R, Rodríguez-Rojas R, del Álamo M, et al. Focused ultrasound subthalamotomy in patients with asymmetric Parkinson's disease: a pilot study. Lancet Neurol. 2018; 17: 54-63.
11. Gabathuler R. Approaches to transport therapeutic drugs across the blood–brain barrier to treat brain diseases. Neurobio Dis. 2010; 37: 48-57.
12. Pardridge W M. Blood–brain barrier delivery. Drug Discov Today. 2007; 12: 54-61.
13. Torchilin V P. Recent advances with liposomes as pharmaceutical carriers. Nat Rev Drug Discov. 2005; 4: 145-60.
14. Pilakka-Kanthikeel S, Atluri V S R, Sagar V, et al. Targeted brain derived neurotropic factors (BDNF) delivery across the blood-brain barrier for neuro-protection using magnetic nano carriers: an in-vitro study. PLoS One. 2013; 8: e62241.
15. Patel T, Zhou J, Piepmeier J M, et al. Polymeric nanoparticles for drug delivery to the central nervous system. Adv Drug Deliv Rev. 2012; 64: 701-5.
16. Ulbrich K, Hekmatara T, Herbert E, et al. Transferrin-and transferrin-receptor-antibody-modified nanoparticles enable drug delivery across the blood-brain barrier (BBB). Eur J Pharm Biopharm. 2009; 71: 251-6.
17. Ni D, Zhang J, Bu W, et al. Dual-targeting upconversion nanoprobes across the blood–brain barrier for magnetic resonance/fluorescence imaging of intracranial glioblastoma. ACS Nano. 2014; 8: 1231-42.
18. Gao X, Qian J, Zheng S, et al. Overcoming the blood–brain barrier for delivering drugs into the brain by using adenosine receptor nanoagonist. ACS Nano. 2014; 8: 3678-89.
19. Deng C X. Targeted drug delivery across the blood-brain barrier using ultrasound technique. Ther Deliv. 2010; 1: 819-48.
20. Qiao R, Jia Q, Hüwel S, et al. Receptor-mediated delivery of magnetic nanoparticles across the blood–brain barrier. ACS Nano. 2012; 6: 3304-10.
21. Chou D K, Krishnamurthy R, Randolph T W, et al. Effects of Tween 20® and Tween 80® on the stability of Albutropin during agitation. J Pharm Sci. 2005; 94: 1368-81.
22. Loos W J, Baker S D, Verweij J, et al. Clinical pharmacokinetics of unbound docetaxel: role of polysorbate 80 and serum proteins. Clin Pharmacol Ther. 2003; 74: 364-71.
23. Tian X H. Enhanced brain targeting of temozolomide in polysorbate-80 coated polybutylcyanoacrylate nanoparticles. Int J Nanomedicine. 2011; 6: 445-52.
24. Koffie R M, Farrar C T, Saidi L J, et al. Nanoparticles enhance brain delivery of blood–brain barrier-impermeable probes for in vivo optical and magnetic resonance imaging. Proc Natl Acad Sci U S A. 2011; 108: 18837-42.
25. Wagner S, Zensi A, Wien S L, et al. Uptake mechanism of ApoE-modified nanoparticles on brain capillary endothelial cells as a blood-brain barrier model. PloS one. 2012; 7: e32568.
26. Gelperina S E, Khalansky A S, Skidan I N, et al. Toxicological studies of doxorubicin bound to polysorbate 80-coated poly (butyl cyanoacrylate) nanoparticles in healthy rats and rats with intracranial glioblastoma. Toxicol Lett. 2002; 126: 131-41.
27. Dasgupta A, Liu M, Ojha T, et al. Ultrasound-mediated drug delivery to the brain: principles, progress and prospects. Drug Discov Today. 2016; 20: 41-8.
28. Carpentier A, Canney M, Vignot A, et al. Clinical trial of blood-brain barrier disruption by pulsed ultrasound. Sci Transl Med. 2016; 8: 343re2.
29. Sheikov N, Mcdannold N, Vykhodtseva N, et al. Cellular mechanisms of the blood-brain barrier opening induced by ultrasound in presence of microbubbles. Ultrasound Med Biol. 2004; 30: 979-89.
30. Tung Y S, Vlachos F, Feshitan J A, et al. The mechanism of interaction between focused ultrasound and microbubbles in blood-brain barrier opening in mice. J Acoust Soc Am. 2011; 130: 3059-67.
31. Yan F, Li X, Jin Q, et al. Therapeutic ultrasonic microbubbles carrying paclitaxel and LyP-1 peptide: preparation, characterization and application to ultrasound-assisted chemotherapy in breast cancer cells. Ultrasound Med Biol. 2011; 37: 768-79.
32. Rosenfeld E. Non-thermal non-cavitational effects of ultrasound. Ultraschall Med. 2003; 24: 40-4.

33. Liang H D, Tang J, Halliwell M. Sonoporation, drug delivery, and gene therapy. Proceedings of the Institution of Mechanical Engineers. J Eng Med. 2010; 224: 343-61.
34. Chen H, Kreider W, Brayman A A, et al. Blood vessel deformations on microsecond time scales by ultrasonic cavitation. Phys Rev Lett. 2011; 106: 034301.
35. Fan CH, Ting CY, Lin CY, Chan HL, Chang YC, Chen YY, et al. Noninvasive, targeted, and non-viral ultrasound-mediated GDNF-plasmid delivery for treatment of parkinson's disease. Nat Sci Rep. 2016; 6: 19579.
36. Gota V S, Maru G B, Soni T G, et al. Safety and pharmacokinetics of a solid lipid curcumin particle formulation in osteosarcoma patients and healthy volunteers. J Agr Food Chem. 2010; 58: 2095-99.
37. Fu W, Zhuang W, Zhou S, et al. Plant-derived neuroprotective agents in Parkinson's disease. Am J Transl Res. 2015; 7: 1189-202.
38. B Mythri R, M Srinivas Bharath M. Curcumin: a potential neuroprotective agent in Parkinson's disease. Cur Pharm Design. 2012; 18: 91-9.
39. Shrikanth Gadad B, K Subramanya P, Pullabhatla S, et al. Curcumin-glucoside, a novel synthetic derivative of curcumin, inhibits α-synuclein oligomer formation: relevance to Parkinson's disease. Cur Pharm Design. 2012; 18: 76-84.
40. Jiang T F, Zhang Y J, Zhou H Y, et al. Curcumin ameliorates the neurodegenerative pathology in A53T α-synuclein cell model of Parkinson's disease through the downregulation of mTOR/p70S6K signaling and the recovery of macroautophagy. J Neuroimmune Pharm. 2013; 8: 356-69.
41. Qualls Z, Brown D, Ramlochansingh C, et al. Protective effects of curcumin against rotenone and salsolinol-induced toxicity: implications for Parkinson's disease. Neurotox Res. 2014; 25: 81-9.
42. Storka A, Vcelar B, Klickovic U, et al. Safety, tolerability and pharmacokinetics of liposomal curcumin (Lipocurc™) in healthy humans. Int J Clin Pharmacol Therapeut. 2015; 53: 54-65.
43. Pan J, Li H, Ma J F, et al. Curcumin inhibition of JNKs prevents dopaminergic neuronal loss in a mouse model of Parkinson's disease through suppressing mitochondria dysfunction. Transl Neurodegener. 2012; 1: 16.
44. Anand P, Kunnumakkara A B, Newman R A, et al. Bioavailability of curcumin: problems and promises. Mol Pharm. 2007; 4: 807-18.
45. Nelson K M, Dahlin J L, Bisson J, et al. The Essential Medicinal Chemistry of Curcumin: Miniperspective. J Med Chem. 2017; 60: 1620-37.
46. Blanco E, Shen H, Ferrari M. Principles of nanoparticle design for overcoming biological barriers to drug delivery. Nat Biotechnol. 2015; 33: 941-51.
47. Liang X, Li X, Yue X, Dai Z. Conjugation of porphyrin to nanohybrid cerasomes for photodynamic therapy of cancer. Angew Chem Int. 2011; 50: 11622-27.
48. Ma Y, Dai Z, Zha Z, Gao Y, Yue X. Selective Antileukemia effect of stabilized nanohybrid vesicles based on cholesteryl succinyl silane. Biomaterials. 2011; 32: 9300-7.
49. Liang X, Gao J, Jiang L, Luo J, Jing L, Li X, Jin Y, Dai Z. Nanohybrid liposomal cerasomes with good physiological stability and rapid temperature responsiveness for high intensity focused ultrasound triggered local chemotherapy of cancer. ACS Nano. 2015; 9:1280-93.
50. Liang X, Li X, Jing L, et al. Design and Synthesis of Lipidic Organoalkoxysilanes for the Self-Assembly of Liposomal Nanohybrid Cerasomes with Controlled Drug Release Properties. Chem-Euro J. 2013; 19: 16113-21.
51. Cao Z, Yue X, Li X, Dai Z. Stabilized magnetic cerasomes for drug delivery. Langmuir. 2013; 29: 14976-83.
52. Yue X, Dai Z. Recent Advances in Liposomal Nanohybrid Cerasomes as Promising Drug Nanocarriers. Adv Colloid Interfac. 2014; 207: 32-42.
53. Cao Z, Yue X, Jin Y, et al. Modulation of release of paclitaxel from composite cerasomes. Colloid Surface B. 2012; 98: 97-104.
54. Kowall N W, Hantraye P, Brouillet E, et al. MPTP induces alpha-synuclein aggregation in the substantia nigra of baboons. Neuroreport. 2000; 11: 211-3.
55. Dauer W, Przedborski S. Parkinson's disease: mechanisms and models. Neuron. 2003; 39: 889-909.
56. Fornai F, Schlüter O M, Lenzi P, et al. Parkinson-like syndrome induced by continuous MPTP infusion: convergent roles of the ubiquitin-proteasome system and α-synuclein. Proc Natl Acad Sci U S A. 2005; 102: 3413-8.
57. Meredith G E, Totterdell S, Potashkin J A, et al. Modeling PD pathogenesis in mice: advantages of a chronic MPTP protocol. Parkinsonism Relat Disord. 2008; 14: S112-5.
58. Gibrat C, Saint-Pierre M, Bousquet M, et al. Differences between subacute and chronic MPTP mice models: investigation of dopaminergic neuronal degeneration and α-synuclein inclusions. J Neurochem. 2009; 109: 1469-82.
59. Vila M, Vukosavic S, Jackson-Lewis V, et al. α-Synuclein Up-Regulation in Substantia Nigra Dopaminergic Neurons Following Administration of the Parkinsonian Toxin MPTP. J Neurochem. 2000; 74: 721-9.
60. Lin C Y, Hsieh H Y, Chen C M, et al. Non-invasive, neuron-specific gene therapy by focused ultrasound-induced blood-brain barrier opening in Parkinson's disease mouse model. J Control Release. 2016; 235: 72-81.
61. Lin C Y, Hsieh H Y, Pitt W G, et al. Focused ultrasound-induced blood-brain barrier opening for non-viral, non-invasive, and targeted gene delivery. J Control Release. 2015; 212: 1-9.
62. Fan C H, Lin C Y, Liu H L, et al. Ultrasound targeted CNS gene delivery for Parkinson's disease treatment. J Control Release. 2017; 261: 246-62

63. Mead B P, Kim N, Miller G W, et al. Novel focused ultrasound gene therapy approach non-invasively restores dopaminergic neuron function in a rat Parkinson's disease model. Nano Lett. 2017; 17: 3533-42
64. Shen Y, Guo J, Chen G, et al. Delivery of liposomes with different sizes to mice brain after sonication by focused ultrasound in the presence of microbubbles. Ultrasound Med Biol. 2016; 42: 1499-511.
65. Zhou Y, Yan H, Xie Q, et al. Simultaneous analysis of dopamine and homovanillic acid by high-performance liquid chromatography with wall-jet/thin-layer electrochemical detection. Analyst. 2013; 138: 7246-53.